THE GLUK4 KAINATE RECEPTOR SUBUNIT REGULATES MEMORY, MOOD, AND EXCITOTOXIC NEURODEGENERATION

E. R. LOWRY, [a] A. KRUYER, [a] E. H. NORRIS, [a]
C. R. CEDERROTH [b] AND S. STRICKLAND [a*]

[a] *Laboratory of Neurobiology & Genetics, The Rockefeller University, 1230 York Avenue, New York, NY 10065, USA*

[b] *Laboratory of Sensory Neuroscience, The Rockefeller University, 1230 York Avenue, New York, NY 10065, USA*

Abstract—Though the GluK4 kainate receptor subunit shows limited homology and a restricted expression pattern relative to other kainate receptor subunits, its ablation results in distinct behavioral and molecular phenotypes. GluK4 knockout mice demonstrated impairments in memory acquisition and recall in a Morris water maze test, suggesting a previously unreported role for kainate receptors in spatial memory. GluK4 knockout mice also showed marked hyperactivity and impaired pre-pulse inhibition, thereby mirroring two of the hallmark endophenotypes of patients with schizophrenia and bipolar disorder. Furthermore, we found that GluK4 is a key mediator of excitotoxic neurodegeneration: GluK4 knockout mice showed robust neuroprotection in the CA3 region of the hippocampus following intrahippocampal injection of kainate and widespread neuroprotection throughout the hippocampus following hypoxia–ischemia. Biochemical analysis of kainate- or sham-treated wild-type and GluK4 knockout hippocampal tissue suggests that GluK4 may act through the JNK pathway to regulate the molecular cascades that lead to excitotoxicity. Together, our findings suggest that GluK4 may be relevant to the understanding and treatment of human neuropsychiatric and neurodegenerative disorders. © 2013 IBRO. Published by Elsevier Ltd. All rights reserved.

Key words: kainate receptor, GluK4, excitotoxicity, memory, schizophrenia, bipolar disorder.

INTRODUCTION

Glutamate is the principal excitatory neurotransmitter in the central nervous system (CNS), and imbalances in glutamatergic transmission have profound behavioral and physiological consequences. Hypoactivity of the glutamatergic system has been implicated in human neuropsychiatric disorders such as schizophrenia, based initially on clinical observations that glutamate antagonists can mimic certain symptoms of the disease (Krystal et al., 1994). Conversely, hyperactivity of the glutamatergic system can result in excitotoxic neurodegeneration, a form of neuronal cell death that often accompanies ischemic stroke (Olney, 1969).

Both normal and pathological aspects of excitatory neurotransmission are contingent upon the interactions between glutamate and its receptors. Three subtypes of ionotropic receptors – *N*-methyl-D-aspartate (NMDA), α-amino-3-hydroxy-5-methyl-4-isoxazolepropionic acid (AMPA), and kainate (KA) – were initially distinguished by the eponymous glutamate homologs for which they show the highest affinity (Lodge, 2009).

KA receptors assemble as tetramers from five subunit types, GluK1–5 (formerly GluR5–7, KA1, and KA2). GluK1–3 has low-affinity agonist binding sites, while GluK4 and GluK5 have high-affinity sites (London and Coyle, 1979; Hampson et al., 1987). Unlike the other KA receptor subunits, which are expressed throughout the CNS (Lerma et al., 2001), GluK4 is expressed primarily within the cornu ammonis 3 (CA3) region of the hippocampus where it co-assembles pre- and post-synaptically with GluK2 (Darstein et al., 2003).

Initial electrophysiological studies using GluK4 knockout mice revealed that GluK4 ablation results in both pre- and post-synaptic signaling deficits within the mossy fiber pathway, in which granule cells from the dentate gyrus (DG) region of the hippocampus project to pyramidal cells in the CA3 (Amaral and Witter, 1989). These changes appear to be independent of the NMDAR system, as the NMDA component is consistent in slices from WT and GluK4/GluK5 double knockouts treated with the kainate receptor antagonist CNQX (Fernandes et al., 2009). The mossy fiber presynaptic fiber volley, when potentiated by KA, is reduced in GluK4 knockout mice relative to wild-type mice (Catches et al., 2012). GluK4 knockout mice also display decreased excitatory postsynaptic current (EPSC) amplitude (Fernandes et al., 2009) and impaired mossy fiber long-term potentiation (LTP) (Catches et al., 2012) – the cellular process that, according to classical

*Corresponding author. Tel: +1-212-327-8705; fax: +1-212-327-8774.

E-mail address: Strickland@rockefeller.edu (S. Strickland).

Abbreviations: ABR, auditory brainstem response; AMPA, α-amino-3-hydroxy-5-methyl-4-isoxazolepropionic acid; ANOVA, analysis of variance; AP-1, activator protein 1; ATF-2, activating transcription factor 2; CA1, cornu ammonis 1; CA2, cornu ammonis 2; CA3, cornu ammonis 3; CNS, central nervous system; CS, conditioned stimulus; DG, dentate gyrus; FJC, Fluorojade C; GAPDH, glyceraldehyde 3-phosphate dehydrogenase; HI, hypoxia–ischemia; JNK, c-Jun N-terminal kinase; KA, kainate; LTP, long-term potentiation; MAP, mitogen-activated protein; MKK4, MAP kinase kinase 4; MLK3, mixed-lineage kinase 3; MWM, Morris water maze; NMDA, *N*-methyl-D-aspartate; PBS, phosphate-buffered saline; PPI, pre-pulse inhibition; PSD-95, post-synaptic density protein-95; SNP, single nucleotide polymorphism; US, unconditioned stimulus; UTR, untranslated region.

Hebbian theory, is thought to underlie learning and memory (Brown et al., 1990). Furthermore, previous studies in which the mossy fiber pathway has been disrupted in mice by chemical inactivation or frank CA3 lesioning have demonstrated the importance of this region in several learning and memory paradigms, including the Morris water maze (MWM) (Stupien et al., 2003; Florian and Roullet, 2004; Kesner, 2007).

There is also mounting evidence from human and animal studies to suggest a role for aberrant GluK4 expression in schizophrenia and bipolar disorder. Expression of the NMDA receptor subunit NMDAR1, the AMPA receptor subunit GluR1, and the KA receptor subunits GluK3 and GluK4 were all found to be decreased at the mRNA level in post-mortem brain tissue from schizophrenics relative to tissue from normal controls (Porter et al., 1997; Sokolov, 1998). Neuroleptic treatment in schizophrenic patients restored subunit expression to normal levels (Sokolov, 1998). Additionally, a genome-wide association study identified separate single-nucleotide polymorphisms (SNPs) in *Grik4*, the gene encoding GluK4, that confer susceptibility to schizophrenia and protection against bipolar disorder, respectively (Pickard et al., 2006). This association study was initially undertaken on the basis of clinical observations in a schizophrenic patient who was found to have a chromosomal breakpoint that disrupted *Grik4* (Pickard et al., 2006).

Prepulse inhibition of acoustic startle (PPI) is a cross-species indicator of sensorimotor gating and involves a suppression of the startle response evoked by a loud tone when that tone is immediately preceded by a weaker tone (Geyer et al., 1990). Under normal conditions, PPI is thought to be a precognitive means of preventing sensory overload (van den Buuse, 2010). Meanwhile, impaired PPI is widely considered to be an endophenotype of schizophrenia – a disorder characterized by cognitive disorganization and an inability to distinguish between salient and non-salient environmental cues (Perry and Braff, 1994). Patients in the manic phase of bipolar disorder also exhibit decreased PPI (Perry et al., 2001).

In addition to its role in memory and behavior, we postulated that GluK4 may also play a role in excitotoxic neurodegeneration. Pyramidal cells in the CA3 are highly – and selectively – vulnerable to cell death (Nadler, 1981; Ben-Ari, 1985) in some models of KA-induced excitotoxicity. Furthermore, KA receptors can couple directly with the c-Jun N-terminal kinase (JNK) pathway, a mitogen-activated protein (MAP) kinase pathway that mediates excitotoxic neurodegeneration (Savinainen et al., 2001). GluK2 and GluK5 subunits form a signaling complex with postsynaptic density protein-95 (PSD-95) and mixed lineage kinase 3 (MLK3), and assembly of this complex under excitotoxic conditions leads to the autophosphorylation of MLK3 and initiation of the phosphorylation cascade that results in JNK pathway activation (Tian et al., 2005; Jiang et al., 2007).

While the intermediate series of molecular events that follows JNK pathway activation and results in neuronal death remains poorly understood, there is strong evidence to suggest that the JNK pathway is crucial in the induction of excitotoxicity: JNK3 knockout mice are resistant to ischemia-induced neurodegeneration (Yang et al., 1997), and JNK pathway inhibitors such as D-JNKI1 have well-documented neuroprotective effects in many models of excitotoxicity (Bogoyevitch et al., 2004).

To investigate the role of GluK4 in excitotoxic neuronal death, we evaluated the extent of cell death in wild-type and GluK4 knockout mice following intrahippocampal KA injections and hypoxia–ischemia (HI), a murine model of stroke. We found that GluK4 ablation was neuroprotective in both paradigms, and that GluK4, like GluK2, may orchestrate neurodegeneration by inducing the JNK pathway.

EXPERIMENTAL PROCEDURES

Generation of GluK4 knockout animals

GluK4 knockout animals were generated by crossing mice homozygous for a *Grik4* allele in which exon 16 was flanked by lox-P sites (generously provided by the Contractor Laboratory at Northwestern University) (Fernandes et al., 2009) with mice homozygous for a transgene encoding Cre-recombinase under the control of an EIIA promoter (The Jackson Laboratory, Bar Harbor, ME, USA). The EIIA promoter is active in the early mouse embryo, allowing for Cre-mediated recombination in many tissues, including germ cells. Animals resulting from this cross transmit the recombined *Grik4* allele to their progeny in a global, Cre-independent manner. The resulting GluK4 knockout animals had a mixed C57Bl/6/129SvE background. Animals homozygous for the wild-type *Grik4* allele but maintained on the same background as GluK4 knockout mice are referred to herein as wild-type mice.

For all experiments, 8- to 12-week-old male mice were maintained on a normal 12-h light/dark cycle from 7:00 am to 7:00 pm with food and water provided *ad libitum*. Breeding pairs were established between male and female mice that were heterozygous for the ablated GluK4 allele to obtain wild-type and GluK4 knockout littermate offspring. Separate cohorts of mice were used for each experiment, with the exception of the open field, PPI, and auditory brainstem response (ABR) experiments. These experiments were performed in the order listed. All procedures were approved by the Institutional Animal Care and Use Committee at the Rockefeller University.

Morris water maze

For this and all subsequent behavioral trials, animals were single-housed in the room in which they were to be tested for at least 5 days prior to the initiation of the trials and handled daily by the experimenters for 1 min per day. All behavioral trials began at 10:00 am. With the exception of the open field test, all behavioral experiments were conducted indoors under standard lighting conditions. Experimenters were blind to the genotype of the animals during handling, testing, and scoring.

MWM experiments were carried out as described previously with slight modifications (Cortes-Canteli et al., 2010). All trials were performed in a 1-m pool filled with room temperature water made opaque with non-toxic white tempera paint. Distal visual cues consisting of black and white geometric shapes were placed throughout the testing room. Mice were subjected to 2 days of visual platform trials (four 1-min trials per day), followed by 4 days of hidden platform trials (four 1-min trials per day). On the last day of the hidden platform trials, mice were

assessed in a 1-min probe trial in which the escape platform was removed from the pool. During the probe trial, animals that have learned to navigate to the platform should spend more time in the quadrant of the pool in which the platform was previously located during the hidden platform trials (target quadrant) than in the other quadrants of the pool. All trials were video-recorded and tracked using Noldus Ethovision XT software (Leesburg, VA, USA). For visual platform trials, latency to reach the platform was compared between genotypes across trial days using a two-way repeated measures analysis of variance (ANOVA). For hidden platform trials, path length was compared across trials between genotypes using a two-way repeated measures ANOVA, and velocity was averaged across all trials for each mouse and compared by Student's *t*-test. Probe trial performance was analyzed by a two-way repeated measures ANOVA for time spent in each quadrant with a Bonferroni post-hoc test.

Open field test

The open field test was conducted in a 46 cm × 46 cm arena placed in a completely dark room. Light meter readings indicated that ambient light levels were 0 lux. The open field chambers (Accuscan, Columbus, OH, USA) were equipped with a laser photobeam tracking system to assess vertical and horizontal beam breaks. Mice were individually placed in the arena and observed for 1 h. Behavior was scored in 5-min bins using Fusion 3.2 Software (Accuscan). Differences in distance traveled over time between wild-type and GluK4-knockout mice were assessed by a two-way repeated measures ANOVA.

Acoustic startle and prepulse inhibition

Mice were tested in SR-LAB startle response system chambers (San Diego Instruments, San Diego, CA, USA), each equipped with a speaker and a Plexiglas restraint tube mounted on a piezoelectric accelerometer unit. Stimuli were presented in blocks, and each stimulus was followed by a non-stimulus period of white noise (background) of 65 dB. In the first block, animals were presented with five single pulses of 120 dB to test their basal startle response. In the second block, animals were presented with 120-dB pulses preceded by a prepulse that was 3, 6, or 12 dB louder than the background. Each prepulse/pulse combination was presented nine times, in pseudo-random order. Single 120-dB pulses were also presented nine times, interspersed with prepulse/pulse pairs. The startle response, Vmax, was recorded using SR-LAB software (San Diego Instruments).

To assess the startle threshold, the startle response to each tone intensity in the second block was averaged for each mouse, and compared between genotypes across tones using a two-way repeated-measures ANOVA with a Bonferroni post-hoc test. The percent PPI was calculated for each prepulse intensity using the following equation: $100 - (($average Vmax for prepulse intensity in question/average Vmax within block 2 for a single 120-dB pulse$) \times 100)$. Percent PPI was compared between genotypes across prepulse intensity by a two-way repeated-measures ANOVA with a Bonferroni post-hoc test.

Auditory brainstem response

Mice were anesthetized for ABR measures with a mixture of ketamine/xylazine (80 mg/kg; 12 mg/kg respectively). The positive needle electrode was inserted subdermally at the vertex; the negative electrode was placed underneath the pinna of the left ear; the ground electrode was placed near the tail. ABRs were evoked within the auditory canal with 5-ms tone pips (0.5 ms rise-fall, cos2 onset, at 30/s). The response was amplified 10,000-fold and filtered from 300 Hz to 3 kHz using an Astro-Med p55 preamplifier (West Warwick, RI, USA). The response was then acquired and averaged using a USB-6210 data acquisition board (National Instruments, Austin, TX, USA) controlled by custom software written in LabVIEW (National Instruments). Sound levels were decreased in 5-dB steps from 100-dB SPL until threshold. One thousand responses were averaged for each sound level. During visual inspection of stacked waveforms, ''threshold'' was defined as the lowest SPL level at which any wave could be detected. Hearing thresholds between genotypes were compared across tone frequencies using a two-way repeated-measures ANOVA.

Stereotaxic injections

Intrahippocampal stereotaxic injections were performed as described (Chen and Strickland, 1997). Animals were anesthetized with 2.5% tribromoethanol (Sigma–Aldrich, St. Louis, MO, USA; 0.02 mL/g of body weight) and atropine (0.6 mg/kg of body weight). Animals were then placed in a stereotaxic apparatus (Stoetling, Wood Dale, IL, USA) and injected over the course of 60 s with 300 nL phosphate-buffered saline (PBS) or 0.15 nmol KA in 300 nL PBS. Injection coordinates relative to Bregma were as follows: −2.5 mm on the anterior–posterior axis; 1.7 mm from the midline on the medial–lateral axis; and 1.7 mm dorsal–ventral from the surface of the skull. For stereology experiments, animals were injected unilaterally. For biochemistry experiments, animals were injected bilaterally. Injections were performed with a 2.5 µL Hamilton syringe equipped with a 33-gauge blunt needle and controlled by an automated microinjection pump (World Precision Instruments, Sarasota, FL, USA). After injection, the needle was retracted 0.1 mm and left in place for 2 min to allow for diffusion of the injected material. Animals were then injected intraperitoneally with 0.03 mL buprenorphine (Reckitt Benckiser Pharmaceuticals, Richmond, VA, USA; 0.03 mg/kg of body weight) for analgesia and 500 mL sterile 0.9% saline for rehydration and allowed to recover on a heating pad.

Hypoxia–ischemia

HI was induced as described with slight modifications (Levine, 1960). Animals were maintained under deep isoflurane anesthesia during surgery. The left common carotid artery was exposed and gently separated from the vagus nerve. The artery was then ligated at two points several millimeters apart with 6-0 silk sutures and transected between the ligation points. Following surgery, the mice were allowed to recover for 40 min. Animals were then transferred to a hypoxic chamber maintained at 8% O_2 and 92% N_2 for 45 min at 37 °C.

Stereology

Twenty-four hours after intrahippocampal injection or HI, animals were perfused with saline and paraformaldehyde, and brains were cryoprotected and frozen as described (Chen and Strickland, 1997). Thin, free-floating sections were collected on a cryostat and stored at −20 °C until use. A subset of sections from each brain were stained with 0.1% Cresyl Violet acetate (Sigma–Aldrich) to assess gross morphology. Sections for stereology were mounted on glass slides and dried overnight at room temperature, then co-stained with Fluorojade C (FJC) and DAPI as described (Schmued et al., 2005), and visualized using an Axiovert 200 inverted epifluorescence microscope (Carl Zeiss, Inc., Thornwood, NY, USA). All sections were imaged at 5× magnification. Exposure time and gain were consistent for each stain between all sections from all animals.

Cell death was quantified using NIH Image J software. Hippocampal subregions were identified and outlined by observation of DAPI staining. Subregion outlines were then

overlaid onto corresponding FJC images. The FJC images were split into their component red, green, and blue color channels, and the green channel was selected for further processing. Images were calibrated in μm, and then thresholded to highlight FJC-positive cells. The area of FJC-positive staining within each hippocampal subregion was recorded and normalized to the total number of slices quantified. Differences in FJC area between genotypes were analyzed for each subregion using a two-tailed Student's t-test.

Western blotting

To investigate the activation of JNK pathway components, animals were injected intrahippocampally with PBS or KA, and killed by cervical dislocation after 24 h. The KA-mediated model of neurodegeneration was chosen over the HI-mediated model because the nature of the insult – KA-induced excitotoxicity – is specific to KA receptors, and the extent of damage is highly reproducible between animals. Hippocampi were quickly removed and microdissected on ice with sterile tools (Lein et al., 2004) to isolate the hippocampal subfields. All dissections were carried out under a dissection microscope to distinguish the anatomical landmarks of the hippocampus, which consist of the upper and lower boundaries of the DG. With the hippocampus oriented such that the medial face is visible, and the dorsal side is up, the CA3 lies below the DG and can be readily isolated by following the boundary of the DG (Lein et al., 2004). In the experiments described herein, the CA3 subregion from one hemisphere of each animal was analyzed. Tissue was immediately frozen in sterile tubes on dry ice and stored at −80 °C until use. Total RNA (for experiments not reported here) and total protein were isolated simultaneously using TRIzol (Life Technologies, Grand Island, NY, USA) according to the manufacturer's instructions.

For Western blotting, 30 μg of CA3 protein per lane were loaded onto a 10% Tris–glycine polyacrylamide gel. Proteins were transferred to a PVDF membrane, and membranes were blocked in 5% milk before overnight incubation in primary antibody at 4 °C. Anti-phosphorylated MAP kinase kinase 4 (MKK4), anti-JNK, anti-phosphorylated JNK, anti-cJun, anti-phosphorylated cJun, and anti-phosphorylated activating transcription factor 2 (ATF-2) antibodies were all purchased from Cell Signaling (Danvers, MA, USA) and used at 1:1000 in the dilution buffer recommended by the manufacturer. Anti c-Fos was purchased from EMD Millipore Calbiochem (Billerica, MA, USA) and used at 1:250 in 5% milk. Following overnight incubation in primary antibody, blots were washed, incubated in the appropriate secondary antibody, washed again, incubated in chemiluminescent reagent (PerkinElmer, Waltham, MA, USA), and exposed to film. Band intensity was quantified using Adobe Photoshop software (San Jose, CA, USA) and normalized to glyceraldehyde 3-phosphate dehydrogenase (GAPDH) (1:2000 in 5% bovine serum albumin; Abcam, Cambridge, MA, USA) from the same blot.

RESULTS

Spatial memory acquisition and recall are impaired in GluK4 knockout mice

To investigate the role of GluK4 in spatial memory, we compared wild-type and GluK4 knockout mice in a MWM test of spatial reference memory. Mice were initially tested in a visual platform paradigm, where the platform was raised above the water surface. No differences in escape latency were observed (two-way ANOVA for latency to reach platform between genotypes across testing days, effect of genotype: $F(1, 23) = 1.15$, $p = 0.2946$; Fig. 1A), suggesting that
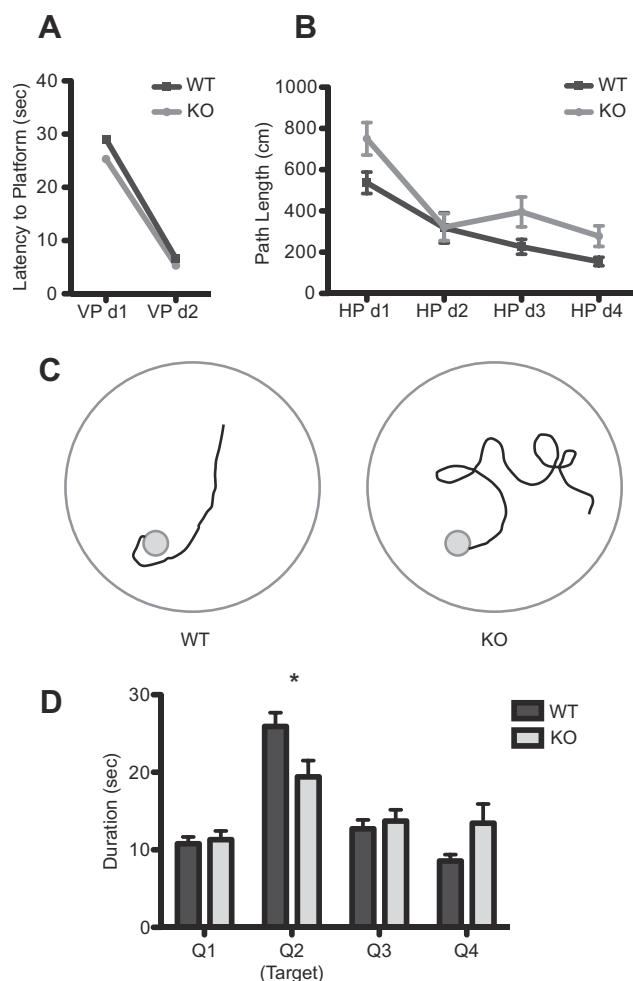

Fig. 1. Spatial memory impairments in GluK4 knockout mice. (A) Wild-type ($n = 13$) and GluK4 knockout mice ($n = 12$) did not differ significantly in their latency to reach the escape platform during the visual platform trials of the MWM, indicating that GluK4 knockout mice had no inherent deficits in vision, swimming ability, or motivation to reach the platform. VP, visual platform. (B) The trajectory to reach the escape platform in hidden platform trials of the MWM was significantly longer in knockout ($n = 12$) versus wild-type mice ($n = 13$), despite overall decreases in path length in both genotypes. HP, hidden platform. (C) Representative traces of search strategies used by wild-type and GluK4 knockout mice on day 4 of hidden platform trials highlight the difference in swim trajectory between wild-type and GluK4 knockout mice. (D) During the probe trial, in which the escape platform was removed from the pool, wild-type mice ($n = 13$) spent significantly more time in the target quadrant than the knockout mice ($n = 12$) did. Data represent mean ± SEM. $^*p < 0.05$.

there were no basal differences between genotypes in visual or swimming abilities or in motivation to escape from the pool.

Both wild-type and GluK4 knockout animals showed progressive decreases in path length between the point of water entry and the escape platform over time. However, the GluK4 knockout cohort performed significantly worse than the wild-type cohort throughout hidden platform testing, demonstrating increased path length (two-way ANOVA for path length between genotypes across testing days, effect of genotype: $F(1, 23) = 5.93$, $p = 0.0231$; effect of time: $F(3, 69) = 25.43$; $p <$

0.0001; Fig. 1B, C) without any concomitant changes in velocity (wild-type mean velocity in cm/s over all hidden platform trials ± SEM = 19.53 ± 0.73, n = 13; knockout mean velocity ± SEM = 20.60 ± 0.45, n = 12; Student's t-test, p = 0.2407).

Following hidden platform training, a probe trial was performed in which the escape platform was removed from the pool. A two-way ANOVA with Bonferroni post-hoc analysis for time spent in each quadrant revealed a significant effect of quadrant ($F(3,92) = 25.63$, $p < 0.0001$), with a significant difference between genotypes in the time spent in the target quadrant ($p < 0.05$) as well as a significant interaction between the genotype and quadrant ($F(3,92) = 4.67$, $p = 0.0044$), indicating that GluK4 knockout mice had decreased preference for the target quadrant when compared with wild-type mice (Fig. 1D). Taken together, our results from the hidden platform and probe trials indicate that GluK4 modulates spatial memory in the MWM.

GluK4 ablation results in hyperactivity

Since increased locomotion is a hallmark of animal models of schizophrenia (van den Buuse, 2010), we investigated locomotor behavior in wild-type versus GluK4 knockout mice in an hour-long open field trial in a dark testing environment. While both wild-type and GluK4 knockout animals initially displayed high levels of activity at the beginning of the trial that progressively decreased as the animals habituated to the novel environment, GluK4 knockout animals traveled consistently greater distances over the course of the trial than wild-type animals (two-way ANOVA for distance traveled: effect of time, $F(11,275) = 31.26$, $p < 0.0001$; effect of genotype: $F(1,25) = 8.43$, $p = 0.0076$; wild-type n = 15, knockout n = 12; Fig. 2A). There was no significant interaction between genotype and time (two-way ANOVA for distance traveled: interaction between time and genotype, $F(11,275) = 0.22$, $p = 0.9963$), indicating that the hyperlocomotion exhibited by the GluK4 knockout animals was independent of habituation, and rather a function of GluK4 ablation.

Sensorimotor gating is impaired in GluK4 knockout mice

PPI is a cross-species test of sensorimotor gating and is reliably impaired in patients with schizophrenia and bipolar disorder (Perry and Braff, 1994; Perry et al., 2001). To assess the effect of GluK4 ablation on PPI, we evaluated wild-type and GluK4 knockout mice in a multi-block PPI paradigm. First, we evaluated the startle response to single broad band white noise pulses of varying intensity, and found significant differences between wild-type and GluK4 knockout mice (two-way ANOVA, effect of genotype, $F = 7.12$, $p = 0.0132$; wild type n = 15, knockout n = 12; Fig. 2B). Post-hoc analysis of the individual pulse intensities revealed that the startle responses to 80, 90, and 100 dB pulses were largely the same between genotypes, but that GluK4 knockout mice displayed significantly impaired startle responses relative to wild-type mice at 110 dB ($p < 0.01$) and 120 dB ($p < 0.0001$). Consistent with a previous
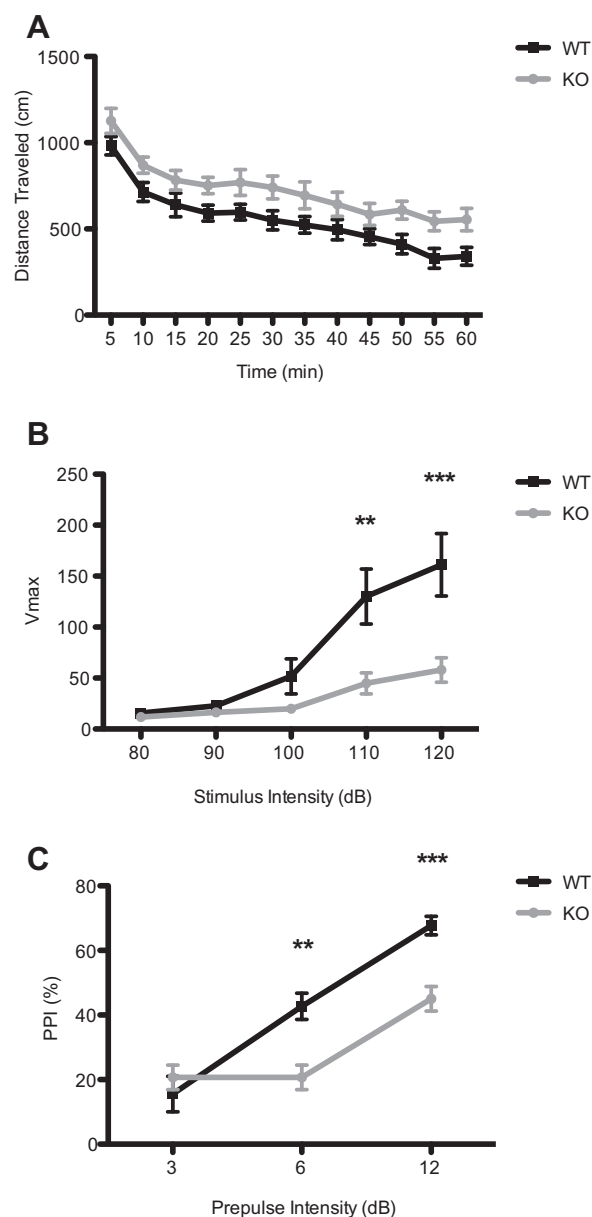
Fig. 2. GluK4 knockout mice display hyperlocomotion and impaired PPI. (A) GluK4 knockout mice (n = 12) traveled significantly greater distances throughout the 1-h open field trial than wild-type mice (n = 15; two-way ANOVA for distance traveled, effect of genotype, $p = 0.0076$), indicating basal hyperactivity. (B) The acoustic startle response was significantly decreased in GluK4 knockout mice (n = 12) relative to wild-type mice (n = 15) at stimulus intensities of 110 and 120 dB. (C) GluK4 knockout mice (n = 12) displayed reduced PPI relative to wild-type mice (n = 15) at pre-pulse tones of 6 and 12 dB above the background, indicating that knockouts had deficits in sensorimotor gating. Data represent mean ± SEM. $^{**}p < 0.01$, $^{***}p < 0.001$.

report (Catches et al., 2012), these findings suggest GluK4 KO mice are less anxious than wild-type animals.

We verified whether the impaired startle response deficit at high intensities observed in GluK4 knockout animals resulted from hearing deficits. We confirmed by means of ABRs, in the same cohort of wild-type and GluK4 knockout animals used in the PPI trials, that hearing was not affected by GluK4 ablation. Hearing

thresholds at 8-, 16-, and 32-kHz frequencies were not significantly different between wild-type and GluK4 knockout animals (wild-type mean hearing threshold in dB at 8, 16, and 32 kHz, respectively: 46.11, 41.11, and 89.44 dB, $n = 9$; knockout mean hearing threshold in dB at 8, 16, and 32 kHz, respectively: 45.00, 33.13, and 89.38 dB, $n = 8$; two-way ANOVA for hearing threshold across tone frequency: effect of genotype, $F(1, 15) = 0.19$, $p = 0.6675$), indicating that hearing remained intact in the absence of GluK4.

Next, a 120-dB pulse was preceded by a prepulse that varied from 3 to 12 dB above a background white noise level of 65 dB. The percent PPI was significantly reduced in GluK4 knockout mice compared to wild-type mice (two-way ANOVA for %PPI across pre-pulse intensities, effect of genotype, $F(1, 25) = 8.52$, $p = 0.0073$; wild-type $n = 15$, knockout $n = 12$; Fig. 2C), indicating that GluK4 mice did not effectively inhibit the startle response following a prepulse. Post-hoc analysis indicated that this effect was significant at a prepulse intensity of 6 dB ($p < 0.01$) and 12 dB ($p < 0.001$) above the background.

GluK4 mediates KA-induced neurodegeneration in the CA3 region of the hippocampus

The CA3 region of the hippocampus is exceptionally vulnerable to excitotoxic neurodegeneration (Nadler, 1981; Ben-Ari, 1985) and represents the region of highest GluK4 expression within the brain (Darstein et al., 2003). To determine the effect of GluK4 deficiency on excitotoxicity, we performed intrahippocampal stereotaxic KA injections (Fig. 3A, B). We found that GluK4 deficiency resulted in significantly reduced KA-induced cell death in the CA3 region (Student's t-test, $p = 0.0271$), but not in the CA1, CA2, or DG (Fig. 3C–G). These results indicate that GluK4 mediates excitotoxic cell death within the CA3.

GluK4 orchestrates widespread neurodegeneration in murine model of ischemia

To further explore the role of GluK4 in neurodegeneration in a clinically relevant context, we compared neurodegeneration in wild-type and GluK4 knockout mice following HI, a murine model of stroke. We found that HI resulted in extensive cell death in all hippocampal subregions in wild-type animals. However, GluK4-deficient animals showed dramatically reduced neurodegeneration throughout the hippocampus relative to wild-type animals (Student's t-test, $p = 0.0405$), particularly in the CA1 (Student's t-test, $p = 0.0371$), CA2 (Student's t-test, $p = 0.0187$), and CA3 subregions (Student's t-test, $p = 0.0189$) (Fig. 3H–J). The robust neuroprotection afforded by GluK4 ablation suggests that GluK4 plays a critical role in the molecular cascades that result in neurodegenerative cell death within the hippocampus as a whole.

GluK4-mediated excitotoxicity coincides with JNK pathway activation

Given its well-established role in excitotoxic neurodegeneration and its association with other KA receptor subunits (Gupta et al., 1996; Borsello et al., 2003; Tian et al., 2005), we hypothesized that the JNK pathway might be involved in coupling GluK4 activation with neurodegeneration. We investigated the expression and phosphorylation states of JNK pathway components by Western blot in KA-injected wild-type and GluK4 knockout CA3 tissue.

The JNK pathway is activated by the phosphorylation of a MAP kinase kinase kinase, such as MLK3, which in turn phosphorylates MKK4 or -7 (Hirai et al., 1997). We found that KA treatment significantly increased MLK3 levels when compared to PBS in wild-type (Student's t-test, $p = 0.007$; Fig. 4A) but not in GluK4 knockout CA3 samples (Student's t-test, $p = 0.139$; Fig. 4A). MLK3 levels were also significantly higher in wild-type CA3 samples after KA treatment than in GluK4 knockout samples after KA treatment (Student's t-test, $p = 0.003$). Like MLK3, phosphorylated MKK4 was also significantly up-regulated in wild-type CA3 samples following KA treatment as compared to PBS treatment (Student's t-test, $p = 0.003$; Fig. 4B), but remained unchanged in CA3 samples from GluK4 knockout mice (Student's t-test, $p = 0.831$; Fig. 4B).

MKKs perpetuate the kinase cascade by phosphorylating one of three JNK isoforms: JNK 1, 2, or 3. JNK 1 and JNK 2 are expressed systemically, and JNK 3 is primarily expressed in neurons (Gupta et al., 1996; Martin et al., 1996). While native JNK 2/3 expression remained unchanged after KA administration when compared between genotypes (wild-type mean JNK 2/3 expression after KA injection ± SEM = 1.216 ± 0.331 (arbitrary units), $n = 3$; knockout mean JNK 2/3 expression after KA injection ± SEM = 1.105 ± 0.111, $n = 3$; Student's t-test, $p = 0.768$), we observed an increase, though not statistically significant, in wild-type levels of phosphorylated JNK 2/3 after KA treatment relative to PBS treatment (Student's t-test, $p = 0.087$; Fig. 4C). However, the increase in phosphorylated JNK 2/3 levels in KA-treated wild-type samples relative to KA-treated GluK4 knockout samples was statistically significant (Student's t-test, $p = 0.007$; Fig. 4C).

Downstream of their activation, phosphorylated JNK isoforms regulate the activity of activator protein 1 (AP-1), a transcription factor that modulates various cellular processes including apoptosis (Whitmarsh and Davis, 1996). AP-1 assembles as a homo- or heterodimer from a number of DNA-binding bZip proteins, including c-Jun, ATF-2, and c-Fos (Whitmarsh and Davis, 1996). We found that native cJun was up-regulated in KA-treated wild-type samples relative to PBS-treated samples (wild-type mean cJun after KA injection ± SEM = 1.578 ± 0.148 (arbitrary units), $n = 3$; wild-type mean cJun after PBS injection ± SEM = 0.478 ± 0.032 (arbitrary units), $n = 3$; Student's t-test, $p = 0.002$), as were phosphorylated cJun and phosphorylated ATF-2 (Student's t-test, $p = 0.011$, and $p = 0.004$, respectively), but remained unchanged between PBS- and KA-treated GluK4 knockout samples (Fig. 4D, E). Though c-Fos expression was not significantly different between KA- and PBS-treated wild-type samples, it was down-regulated in KA-treated GluK4 knockout samples relative
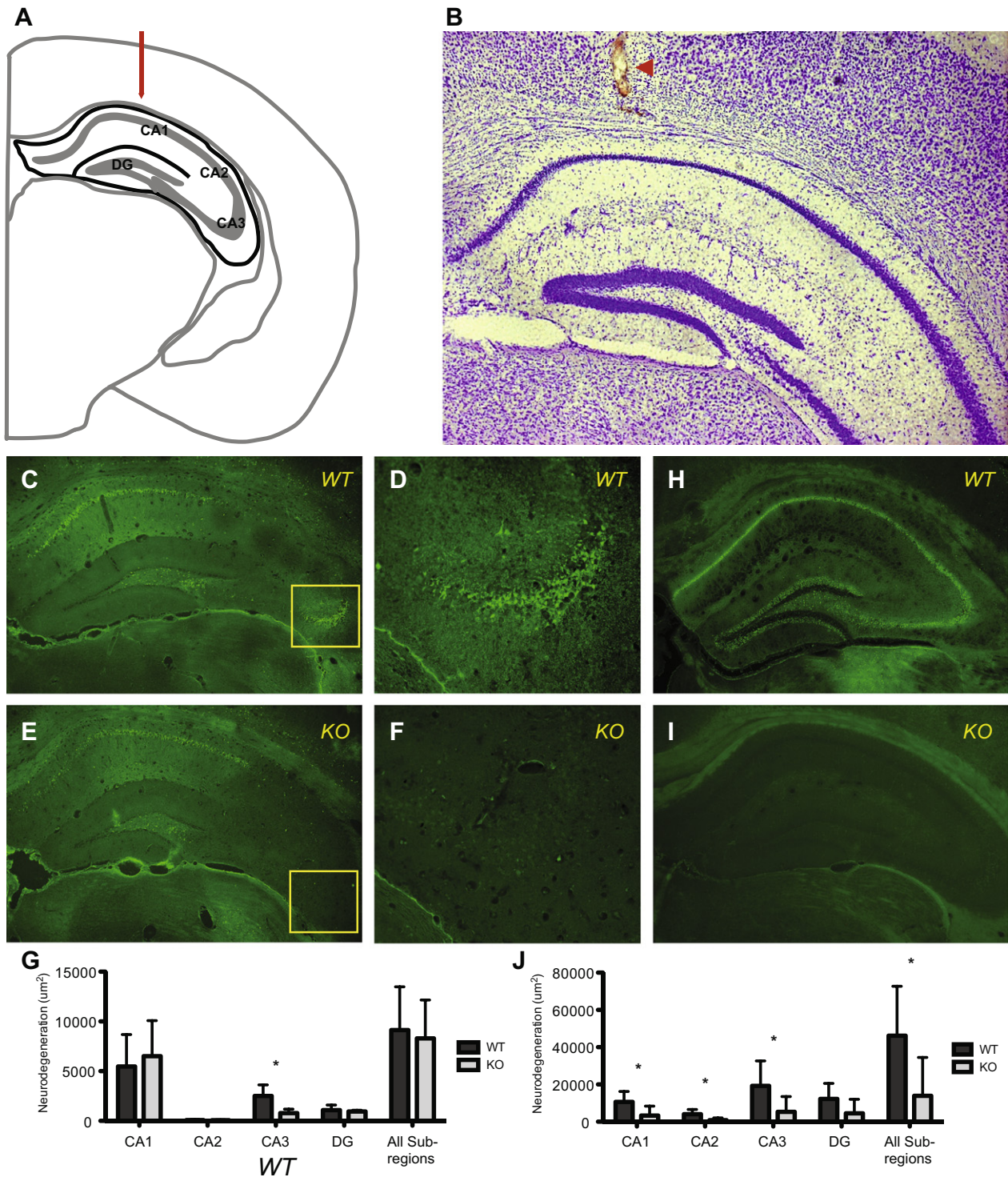
Fig. 3. GluK4 ablation attenuates KA-induced neurodegeneration in the CA3 region of the hippocampus and HI-induced neurodegeneration throughout the hippocampus. (A) Schematic of intrahippocampal injection coordinates in coronal view at Bregma −2.5 mm, adapted from Franklin and Paxinos (2012). Hippocampus is outlined in black. The medial–lateral and dorsal–ventral injection coordinates are indicated by a red arrow. (B) Representative Nissl stain of KA-injected tissue. Red arrowhead indicates injection tract. (C) FJC-stained tissue from KA-treated wild-type animals ($n = 4$) revealed neurodegeneration throughout the hippocampus. (D) The CA3 region of the hippocampus was particularly vulnerable to neurodegeneration in wild-type tissue (enlargement of indicated region of C). (E) Neurodegeneration was decreased in GluK4 knockout tissue, specifically in the CA3 region of the hippocampus (F, enlargement of indicated region of E). (G) Stereological quantification of neurodegeneration, corresponding to the mean area of FJC staining, demonstrated specific neuroprotection of the CA3 region in GluK4 knockout mice. (H) HI, like KA treatment, resulted in extensive neurodegeneration throughout the hippocampus of wild-type animals ($n = 6$) as indicated by FJC. (I) Hippocampal neurodegeneration was strongly reduced in GluK4 knockout animals ($n = 6$). (J) Stereological quantification of neurodegeneration reflects neuroprotection throughout the hippocampus in GluK4 knockout animals relative to wild-type animals after HI. Bars represent mean ± SEM. *$p < 0.05$.
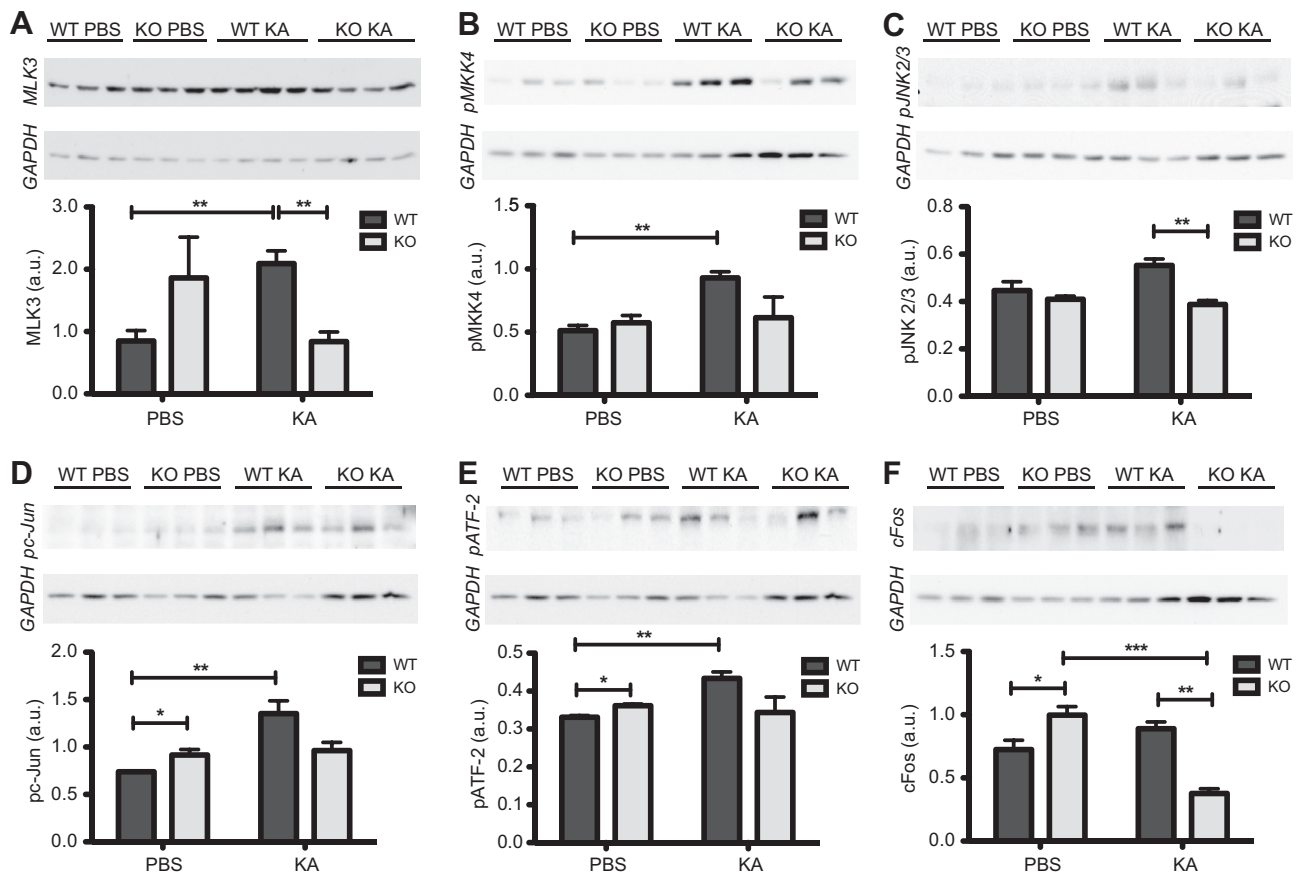
Fig. 4. GluK4 bi-directionally modulates JNK pathway activation to regulate neurodegeneration. (A) MLK3, one of the earliest kinases in the JNK kinase cascade, was up-regulated in wild-type CA3 tissue after KA treatment relative to PBS treatment, but not in GluK4 knockout tissue. MLK3 levels were also significantly higher in wild-type CA3 tissue after KA treatment than in GluK4 knockout tissue after KA treatment. (B) The phosphorylated (activated) form of MKK4, which is downstream of MLK3 in the JNK kinase cascade, was up-regulated in wild-type CA3 tissue after KA treatment relative to PBS treatment, but not in GluK4 knockout CA3 tissue. (C) The phosphorylated, neuronal form of JNK (JNK 2/3, 54 kDa) is up-regulated in KA-treated wild-type tissue relative to KA-treated GluK4 knockout tissue. (D) The phosphorylated form of cJun, a member of the AP-1 transcription factor complex that is activated downstream of JNK, was up-regulated in KA- versus PBS-treated wild-type tissue but not GluK4 knockout tissue. However, phosphorylated c-Jun expression was higher after PBS treatment in GluK4 knockout tissue than in wild-type tissue. (E) Phosphorylated ATF-2, another member of the AP-1 complex, followed a similar expression pattern to phosphorylated cJun. Phosphorylated ATF-2 was up-regulated in KA- versus PBS-treated wild-type tissue but not GluK4 knockout tissue, though its expression was higher after PBS treatment in GluK4 knockout tissue than in wild-type tissue. (F) cFos is also a member of the AP-1 transcription complex. Its expression was strongly down-regulated between KA-treated wild-type and GluK4 knockout tissue, and between PBS- and KA-treated GluK4 knockout tissues. As with the other members of the AP-1 complex, c-Fos expression was increased at the baseline in PBS-treated GluK4 knockout versus wild-type tissue. For all Western blot analyses, $n = 3$ samples per genotype per treatment, except in A where $n = 4$ in the KA treatment group. GAPDH loading controls were included for each blot. Bars represent mean ± SEM. $^*p < 0.05$, $^{**}p < 0.01$, $^{***}p < 0.001$.

to PBS-treated GluK4 knockout samples and KA-treated wild-type samples (Student's t-test, $p = 0.001$ and $p = 0.053$, respectively; Fig. 4F). Surprisingly, phosphorylated c-Jun, phosphorylated ATF-2, and c-Fos levels were all constitutively higher in PBS-treated GluK4 knockout samples than in PBS-treated wild-type samples (Student's t-test, $p = 0.044$, $p = 0.048$, $p = 0.038$, and $p = 0.053$, respectively; Fig. 4D–F). The same trend was observed in MLK3 expression, but was not statistically significant (Fig. 4A). GluK4 may therefore play a role in suppressing JNK pathway activation in non-pathological contexts.

DISCUSSION

GluK4 is critical for learning and memory

While a previous study on GluK4 knockout mice showed that they have no working memory impairment in a spontaneous alternation Y-maze task (Catches et al., 2012), we sought to investigate the role of GluK4 in other forms of memory. We found that GluK4 knockout mice showed deficits in spatial memory acquisition and recall. Though our findings are consistent with previous reports of electrophysiological impairments in GluK4 knockout mice (Fernandes et al., 2009; Catches et al., 2012), we are the first to directly implicate GluK4 – and KA receptors in general – in the generation of spatial memory.

The spatial memory deficits observed in GluK4 knockout mice may also have broader implications for human neuropsychiatric disorders. The MWM task is hippocampus-dependent, and there have been many studies linking schizophrenia with deficits in hippocampus-dependent forms of memory, such as declarative memory (Tamminga et al., 2010). Furthermore, in a computerized, virtual MWM task

adapted for humans, the performance of schizophrenic patients was strikingly similar to that which we observed in GluK4 knockout mice: schizophrenic patients showed no impairments in visual platform trials, but demonstrated increased path length in hidden platform trials and spent less time in the target quadrant during a probe trial (Hanlon et al., 2006).

GluK4 ablation results in phenotypic hallmarks of bipolar disorder and schizophrenia

There is long-standing evidence to support the involvement of abnormal glutamatergic transmission in the pathophysiology of schizophrenia (reviewed most recently by Inta et al., 2010) as well as a growing body of genome-wide association studies to support a specific role for GluK4 (Pickard et al., 2006, 2008). These same studies have also indicated a role for GluK4 in bipolar disorder. GluK4 knockout mice have previously been shown to be less anxious and less despairing, and therefore more risk-inclined, than wild-type mice (Catches et al., 2012), a behavioral hallmark of bipolar disorder in humans. Furthermore, mice deficient in GluK2, the KA receptor subunit with which GluK4 co-assembles (Darstein et al., 2003), show phenotypic traits such as increased aggression and hypersensitivity to amphetamines that parallel the behavior of patients in the manic phase of bipolar disorder (Shaltiel et al., 2008), further suggesting a role for GluK4 in these behavioral processes.

While the etiological underpinnings of schizophrenia and bipolar disorder are complex and difficult to model definitively in animals, the behavioral changes that we observed in GluK4 knockout mice relative to wild-type mice may phenocopy certain facets of these diseases. Hyperlocomotion in animal models of psychological disorders is often considered to be a reflection or behavioral correlate of psychomotor agitation, an endophenotype of both bipolar disorder and schizophrenia (van den Buuse, 2010). According to the dopamine hypothesis of schizophrenia, psychomotor agitation and other positive symptoms of schizophrenia can be attributed to excess dopaminergic activity, and drugs that enhance dopamine neurotransmission, such as amphetamines, induce hyperactivity in rodents (van den Buuse, 2010). Meanwhile, the glutamate hypothesis of schizophrenia postulates that the positive symptoms of schizophrenia are related to insufficient glutamatergic activity, and NMDA receptor antagonists such as MK-801 and phencyclidine also induce hyperactivity in rodents, as does GluK2 ablation (Shaltiel et al., 2008; Gunduz-Bruce, 2009). Thus, hyperlocomotion in GluK4 knockout mice may be relevant to the role of GluK4 in neuropsychiatric disorders.

Furthermore, the hyperlocomotion that we observed in GluK4 knockout mice was specific to the open field test and did not appear to be a confounding factor in our other behavioral assays, particularly the MWM. GluK4 knockout mice showed no deficits in visual platform performance relative to wild-type mice; it was only when the navigation and spatial learning components were introduced in the hidden platform and probe trials that the disparity between GluK4 knockout and wild-type performance became apparent.

It should also be noted that a previous study reported no hyperlocomotion in GluK4 knockout animals in a similar open field assay (Catches et al., 2012). In light of the fact that these same authors report that GluK4 knockout mice show decreased basal levels of anxiety (Catches et al., 2012), it is possible that other experimental variables, such as lighting and mouse handling, affected the locomotion of wild-type and GluK4 knockout animals. Wild-type animals with increased anxiety, brought on by bright lighting or physical handling, may have exhibited increased locomotion, while the decreased basal level of anxiety brought about by GluK4 ablation may have obviated the effect in the knockout cohort.

The involvement of GluK4 in schizophrenia and bipolar disorder is further supported by data from the PPI assays. Compared to wild-type mice, GluK4 knockout mice showed decreased inhibition of the acoustic startle response when the startle-inducing tone was preceded by a weaker tone. Deficits in PPI are common in patients with schizophrenia and have also been observed in patients with bipolar disorder during periods of acute psychotic mania (Perry et al., 2001). The relationship between PPI and psychosis is not fully understood. However, PPI deficits may be a reflection of the fact that such patients are unable to discriminate between trivial and salient stimuli within their environment, and are therefore subjected to constant cognitive overload as they respond to each with equal measure (Perry and Braff, 1994; Geyer et al., 2002). Though measuring psychosis and cognitive overload in animals remains challenging, GluK4 ablation directly phenocopies a human correlate of these dysfunctions by inducing PPI impairments in GluK4 knockout mice.

GluK4 interacts with the JNKK pathway to promote neurodegeneration

Excitotoxicity is responsible for the widespread cell death that underlies many of the debilitating aspects of neurodegenerative diseases such as ischemic stroke. We observed that the CA3 region of the hippocampus in GluK4 knockout animals is protected against neurodegeneration following KA-induced excitotoxicity. This finding is consistent with the fact that GluK4 expression is concentrated in the CA3 (Darstein et al., 2003).

We also observed decreased activation throughout the JNK pathway in GluK4 knockout mice relative to wild-type mice following KA treatment, indicating a possible role for GluK4 in the activation of the JNK pathway under excitotoxic conditions. Conversely, we observed increased activation of AP-1 transcription factor proteins ATF-2, c-Jun, and c-Fos in GluK4 knockout mice relative to wild-type mice at baseline, suggesting that GluK4 may serve to suppress JNK pathway activity under normal conditions. Collectively, these data suggest that GluK4 may regulate or interact with JNK pathway components in a biphasic, context-dependent manner.

Several scenarios present themselves as to how GluK4 and the JNK pathway interact. One possibility is that GluK4 interacts with the JNK pathway directly by participating in heteromeric receptor complexes with GluK2, and, by extension, the GluK2/PSD-95/MLK3 signaling complex that activates the JNK pathway (Tian et al., 2005). GluK4 may also participate in other non-canonical, metabotropic actions that indirectly induce the JNK pathway. The JNK pathway has many upstream effectors, including G-proteins (Yang et al., 2006), and KA receptors are known to couple with G-proteins to mediate various cellular signaling events, such as pre-synaptic glutamate and GABA release (Rodríguez-Moreno and Sihra, 2011; Sihra and Rodríguez-Moreno, 2011). It is also possible that GluK4 serves a purely ionotropic function in the initiation of excitotoxic cell death: post-synaptic GluK4-containing receptors may flux calcium directly into post-synaptic cells, or pre-synaptic GluK4-containing autoreceptors may potentiate the release of excess glutamate from presynaptic cells, and thereby activate any or all forms of post-synaptic ionotropic glutamate receptors. Calcium ions can initiate a large number of signal transduction pathways, and elevated intracellular calcium levels have been shown to induce JNK pathway activation in macrophages (Kim and Sharma, 2004). Further research is warranted into the mechanisms by which GluK4 interacts with the JNK pathway and promotes excitotoxicity.

In contrast to the regionalized neuroprotection that we observed in GluK4 knockout mice following KA-induced excitotoxicity, the neuroprotection observed following HI extended throughout the hippocampus. One explanation for this phenomenon could be that, in the context of HI, GluK4 activates cell death pathways other than, or in addition to, the JNK pathway. These pathways may be more pervasive than the JNK pathway, or they may incite alternative forms of cell death. Ultimately, the profound difference in HI-induced neurodegeneration between wild-type and GluK4 knockout mice suggests that GluK4 is an early and crucial mediator of ischemic brain damage.

CONCLUSIONS

Our findings shed light on the role of GluK4 in the CNS, which, until now, has remained poorly understood. This work reveals that a single glutamate receptor subunit with very limited expression serves as a key modulator of memory, cognition, and baseline affect, on one hand, and excitotoxic cell death cascades on the other, and thus provides critical insight into the mechanisms and potential treatment of human neuropsychiatric and neurodegenerative disorders.

REFERENCES

Amaral DG, Witter MP (1989) The three-dimensional organization of the hippocampal formation: a review of anatomical data. Neuroscience 31:571–591.

Ben-Ari Y (1985) Limbic seizure and brain damage produced by kainic acid: mechanisms and relevance to human temporal lobe epilepsy. Neuroscience 14:375–403.

Bogoyevitch MA, Boehm I, Oakley A, Ketterman AJ, Barr RK (2004) Targeting the JNK MAPK cascade for inhibition: basic science and therapeutic potential. Biochim Biophys Acta 1697:89–101.

Borsello T, Clarke PGH, Hirt L, Vercelli A, Repici M, Schorderet DF, Bogousslavsky J, Bonny C (2003) A peptide inhibitor of c-Jun N-terminal kinase protects against excitotoxicity and cerebral ischemia. Nat Med 9:1180–1186.

Brown TH, Kairiss EW, Keenan CL (1990) Hebbian synapses: biophysical mechanisms and algorithms. Annu Rev Neurosci 13:475–511.

Catches JS, Xu J, Contractor A (2012) Genetic ablation of the GluK4 kainate receptor subunit causes anxiolytic and antidepressant-like behavior in mice. Behav Brain Res 228:406–414.

Chen ZL, Strickland S (1997) Neuronal death in the hippocampus is promoted by plasmin-catalyzed degradation of laminin. Cell 91:917–925.

Cortes-Canteli M, Paul J, Norris EH, Bronstein R, Ahn HJ, Zamolodchikov D, Bhuvanendran S, Fenz KM, Strickland S (2010) Fibrinogen and beta-amyloid association alters thrombosis and fibrinolysis: a possible contributing factor to Alzheimer's disease. Neuron 66:695–709.

Darstein M, Petralia RS, Swanson GT, Wenthold RJ, Heinemann SF (2003) Distribution of kainate receptor subunits at hippocampal mossy fiber synapses. J Neurosci 23:8013–8019.

Fernandes HB, Catches JS, Petralia RS, Copits BA, Xu J, Russell TA, Swanson GT, Contractor A (2009) High-affinity kainate receptor subunits are necessary for ionotropic but not metabotropic signaling. Neuron 63:818–829.

Florian C, Roullet P (2004) Hippocampal CA3-region is crucial for acquisition and memory consolidation in Morris water maze task in mice. Behav Brain Res 154:365–374.

Franklin KBJ, Paxinos G (2008) The mouse brain in stereotaxic coordinates. Amsterdam; London: New York: Elsevier Academic Press.

Geyer MA, McIlwain KL, Paylor R (2002) Mouse genetic models for prepulse inhibition: an early review. Mol Psychiatry 7:1039–1053.

Geyer MA, Swerdlow NR, Mansbach RS, Braff DL (1990) Startle response models of sensorimotor gating and habituation deficits in schizophrenia. Brain Res Bull 25:485–498.

Gunduz-Bruce H (2009) The acute effects of NMDA antagonism: from the rodent to the human brain. Brain Res Rev 60:279–286.

Gupta S, Barrett T, Whitmarsh AJ, Cavanagh J, Sluss HK, Dérijard B, Davis RJ (1996) Selective interaction of JNK protein kinase isoforms with transcription factors. EMBO J 15:2760–2770.

Hampson DR, Huie D, Wenthold RJ (1987) Solubilization of kainic acid binding sites from rat brain. J Neurochem 49:1209–1215.

Hanlon FM, Weisend MP, Hamilton DA, Jones AP, Thoma RJ, Huang M, Martin K, Yeo RA, Miller GA, Cañive JM (2006) Impairment on the hippocampal-dependent virtual Morris water task in schizophrenia. Schizophr Res 87:67–80.

Hirai SI, Katoh M, Terada M, Kyriakis JM, Zon LI, Rana A, Avruch J, Ohno S (1997) MST/MLK2, a member of the mixed lineage kinase family, directly phosphorylates and activates SEK1, an activator of c-Jun N-terminal kinase/stress-activated protein kinase. J Biol Chem 272:15167–15173.

Inta D, Monyer H, Sprengel R, Meyer-Lindenberg A, Gass P (2010) Mice with genetically altered glutamate receptors as models of schizophrenia: a comprehensive review. Neurosci Biobehav Rev 34:285–294.

Jiang H-X, Guan Q-H, Pei D-S, Zhang G-Y (2007) Functional cooperation between KA2 and GluR6 subunits is involved in the ischemic brain injury. J Neurosci Res 85:2960–2970.

Kesner RP (2007) Behavioral functions of the CA3 subregion of the hippocampus. Learn Mem 14:771–781.

Kim J, Sharma RP (2004) Calcium-mediated activation of c-Jun NH2-terminal kinase (JNK) and apoptosis in response to cadmium in murine macrophages. Toxicol Sci 81:518–527.

Krystal JH, Karper LP, Seibyl JP, Freeman GK, Delaney R, Bremner JD, Heninger GR, Bowers MB, Charney DS (1994) Subanesthetic effects of the noncompetitive NMDA antagonist, ketamine, in humans. Psychotomimetic, perceptual, cognitive, and neuroendocrine responses. Arch Gen Psychiatry 51:199–214.

Lein ES, Zhao X, Gage FH (2004) Defining a molecular atlas of the hippocampus using DNA microarrays and high-throughput in situ hybridization. J Neurosci 24:3879–3889.

Lerma J, Paternain AV, Rodríguez-Moreno A, López-García JC (2001) Molecular physiology of kainate receptors. Physiol Rev 81:971–998.

Levine S (1960) Anoxic–ischemic encephalopathy in rats. Am J Pathol 36:1–17.

Lodge D (2009) The history of the pharmacology and cloning of ionotropic glutamate receptors and the development of idiosyncratic nomenclature. Neuropharmacology 56:6–21.

London ED, Coyle JT (1979) Specific binding of [^{3}H]kainic acid to receptor sites in rat brain. Mol Pharmacol 15:492–505.

Martin JH, Mohit AA, Miller CA (1996) Developmental expression in the mouse nervous system of the p493F12 SAP kinase. Brain Res Mol Brain Res 35:47–57.

Nadler JV (1981) Minireview. Kainic acid as a tool for the study of temporal lobe epilepsy. Life Sci 29:2031–2042.

Olney JW (1969) Brain lesions, obesity, and other disturbances in mice treated with monosodium glutamate. Science 164:719–721.

Perry W, Braff DL (1994) Information-processing deficits and thought disorder in schizophrenia. Am J Psychiatry 151:363–367.

Perry W, Minassian A, Feifel D, Braff DL (2001) Sensorimotor gating deficits in bipolar disorder patients with acute psychotic mania. Biol Psychiatry 50:418–424.

Pickard BS, Knight HM, Hamilton RS, Soares DC, Walker R, Boyd JKF, Machell J, Maclean A, McGhee KA, Condie A, Porteous DJ, St Clair D, Davis I, Blackwood DHR, Muir WJ (2008) A common variant in the 3′UTR of the GRIK4 glutamate receptor gene affects transcript abundance and protects against bipolar disorder. Proc Natl Acad Sci U S A 105:14940–14945.

Pickard BS, Malloy MP, Christoforou A, Thomson PA, Evans KL, Morris SW, Hampson M, Porteous DJ, Blackwood DHR, Muir WJ (2006) Cytogenetic and genetic evidence supports a role for the kainate-type glutamate receptor gene, GRIK4, in schizophrenia and bipolar disorder. Mol Psychiatry 11:847–857.

Porter RH, Eastwood SL, Harrison PJ (1997) Distribution of kainate receptor subunit mRNAs in human hippocampus, neocortex and cerebellum, and bilateral reduction of hippocampal GluR6 and KA2 transcripts in schizophrenia. Brain Res 751:217–231.

Rodríguez-Moreno A, Sihra TS (2011) Metabotropic actions of kainate receptors in the control of glutamate release in the hippocampus. Adv Exp Med Biol 717:39–48.

Savinainen A, Garcia EP, Dorow D, Marshall J, Liu YF (2001) Kainate receptor activation induces mixed lineage kinase-mediated cellular signaling cascades via post-synaptic density protein 95. J Biol Chem 276:11382–11386.

Schmued LC, Stowers CC, Scallet AC, Xu L (2005) Fluoro-Jade C results in ultra high resolution and contrast labeling of degenerating neurons. Brain Res 1035:24–31.

Shaltiel G, Maeng S, Malkesman O, Pearson B, Schloesser RJ, Tragon T, Rogawski M, Gasior M, Luckenbaugh D, Chen G, Manji HK (2008) Evidence for the involvement of the kainate receptor subunit GluR6 (GRIK2) in mediating behavioral displays related to behavioral symptoms of mania. Mol Psychiatry 13:858–872.

Sihra TS, Rodríguez-Moreno A (2011) Metabotropic actions of kainate receptors in the control of GABA release. Adv Exp Med Biol 717:1–10.

Sokolov BP (1998) Expression of NMDAR1, GluR1, GluR7, and KA1 glutamate receptor mRNAs is decreased in frontal cortex of "neuroleptic-free" schizophrenics: evidence on reversible up-regulation by typical neuroleptics. J Neurochem 71:2454–2464.

Stupien G, Florian C, Roullet P (2003) Involvement of the hippocampal CA3-region in acquisition and in memory consolidation of spatial but not in object information in mice. Neurobiol Learn Mem 80:32–41.

Tamminga C, Stan A, Wagner A (2010) The hippocampal formation in schizophrenia. Am J Psychiatry 167:1178–1193.

Tian H, Zhang Q-G, Zhu G-X, Pei D-S, Guan Q-H, Zhang G-Y (2005) Activation of c-Jun NH2-terminal kinase 3 is mediated by the GluR6.PSD–95.MLK3 signaling module following cerebral ischemia in rat hippocampus. Brain Res 1061:57–66.

van den Buuse M (2010) Modeling the positive symptoms of schizophrenia in genetically modified mice: pharmacology and methodology aspects. Schizophr Bull 36:246–270.

Whitmarsh AJ, Davis RJ (1996) Transcription factor AP-1 regulation by mitogen-activated protein kinase signal transduction pathways. J Mol Med 74:589–607.

Yang DD, Kuan CY, Whitmarsh AJ, Rincón M, Zheng TS, Davis RJ, Rakic P, Flavell RA (1997) Absence of excitotoxicity-induced apoptosis in the hippocampus of mice lacking the Jnk3 gene. Nature 389:865–870.

Yang L, Mao L, Chen H, Catavsan M, Kozinn J, Arora A, Liu X, Wang JQ (2006) A signaling mechanism from G alpha q-protein-coupled metabotropic glutamate receptors to gene expression: role of the c-Jun N-terminal kinase pathway. J Neurosci 26:971–980.